To be published in the Proceedings
of the Soviet-American Symposium
on Theory of Light Scattering in
Solids, Moscow, USSR,
May 26 - 30, 1975

LBL-4170

Conf-750582--1

RESONANT RAMAN SCATTERING NEAR EXCITONIC TRANSITIONS

Y. R. Shen

September, 1975

Prepared for the U. S. Energy Research and
Development Administration under Contract W-7405-ENG-48

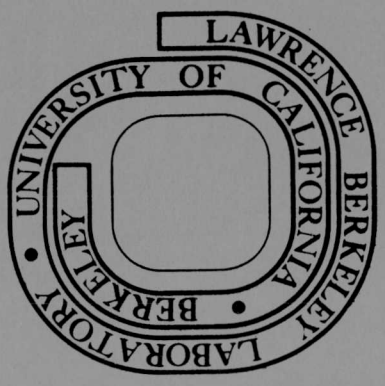

LBL-4170

To appear in the Proceedings of the Soviet-American Symposium on Theory of Light Scattering in Solids. Moscow, May 26-30, 1975.

LBL-4170
Preprint

UNIVERSITY OF CALIFORNIA

Lawrence Berkeley Laboratory
Berkeley, California
AEC Contract No. W-7405-eng-48

RESONANT RAMAN SCATTERING NEAR EXCITONIC TRANSITIONS

Y. R. Shen

September, 1975

LBL-4170

RESONANT RAMAN SCATTERING NEAR EXCITONIC TRANSITIONS

by

Y. R. Shen

Department of Physics, University of California

and

Inorganic Materials Research Division

Lawrence Berkeley Laboratory, Berkeley, California 94720

Resonant Raman Scattering Near Excitonic Transitions

Y. R. Shen
Department of Physics, University of California, and
Inorganic Materials Research Division,
Lawrence Berkeley Laboratory, Berkeley, California 94720

ABSTRACT

We use the cases of Cu_2O in MnF_2 to illustrate the principles and usefulness of the resonant Raman technique. We show that the resonant Raman results can give not only a better understanding of the phonon (magnon) structure but also more details about the excitonic structure and the coupling between excitons (or electrons and holes) and phonons (magnons).

INTRODUCTION

The advent of tunable dye lasers has led the field of Raman spectroscopy into a new era. With the incoming laser frequency variable around particular electronic excitations, Raman scattering in solids can now yield not only better understanding of phonon structure, but also detailed information about electronic structure and electron-phonon interaction for the specific electronic excitations. Over the past three years, resonant Raman scattering (RRS) work has been carried out in a number of solids. In each case, the results are interesting and exciting. We do not have space here to discuss all these interesting cases. Instead, I have decided to choose RRS in Cu_2O as an example to illustrate the RRS technique. Cu_2O is the well-known semiconductor which led to the first junction diodes. It is also the most frequently quoted crystal for exhibiting clear, well-defined series of excitonic transitions. The late Professor E. F. Gross had made great contribtuion to the understanding of the excitonic properties in Cu_2O. Here, we shall show that by RRS, we can now learn even more about the excitonic properties, such as the exciton mass and exciton lifetime. In addition, we can also obtain a thorough understanding of the phonon spectra of Cu_2O and detailed information about phonon dispersion and exciton-phonon interaction in Cu_2O.[2-4]

Resonant Raman study can of course be extended to other elementary excitations besides phonons. As an example, we shall also discuss

briefly here the case of RRS by magnons in MnF_2.[5] In some respects, this case is a close analog of RRS by phonons in Cu_2O.

Background Information on Cu_2O

The crystal structure of Cu_2O is shown in Fig. 1. It is a cubic lattice with 6 atoms per unit cell and an O_h^4 space group. From group theoretical analysis, we expect to find the following zone-center optical phonons: 6 infrared active ones, $\Gamma_{15}^{-(1)}(3)$ and $\Gamma_{15}^{-(2)}(3)$, 3 Raman active ones, $\Gamma_{25}^{+}(3)$, and 6 silent ones, $\Gamma_{2}^{-}(1)$, $\Gamma_{12}^{-}(2)$, and $\Gamma_{25}^{-}(3)$. The frequencies of these modes have been obtained by various methods, including RRS, as shown in Table I. All these modes have definite parities because of inversion symmetry of the crystal.

An off-resonant Raman spectrum of Cu_2O is shown in Fig. 2.[6] This spectrum was taken with a Kr ion laser at 6471 Å, which is about 1050 cm^{-1} below the first exciton absorption line or 2200 cm^{-1} below the band gap. Intuitively, one would expect the spectrum to be dominated by the only Raman-active mode $\Gamma_{25}^{+}(3)$ at 515 cm^{-1}. However, the spectrum of Fig. 2 actually consists of a large number of sharp lines; the expected Raman-active mode, on the other hand, does not even show up. This indicates that the usual off-resonant selection rules are not operative here and multiphonon modes must have dominated the spectrum. As we shall see later, such a Raman spectrum can be understood only with the help of RRS.

In RRS measurements, we tune the incoming laser frequency around optical absorption lines or bands. The absorption spectrum of Cu_2O near the absorption edge is shown in Fig. 3a. It consists of four series of

of sharp lines superimposed on a continuum. The four series of sharp lines are the well-known exciton series formed by electrons of the two lowest conduction bands and holes of the two top valence bands as shown in Fig. 3b.[7] The first series is known as the yellow exciton series. By the parity selection rule, electric-dipole excitation of the 1s yellow exciton is forbidden; the electric-quadrupole excitation is responsible for the observed 1s line. However, electric-dipole excitation of the forbidden 1s exciton becomes allowed with the assistence of an odd-parity phonon. This phonon-assisted excitation of the 1s yellow exciton leads to the absorption continuum in Fig. 3a. The phonon which contributes most to the continuum is the Γ_{12}^{-} mode. This explains why the absorption continuum begins at 110 cm^{-1} above the 1s yellow exciton line at $\omega_{1s}(o)$ and has a frequency dependence $[\omega - \omega_{1s}(o) - \omega(\Gamma_{12}^{-})]^{1/2}$ near the absorption edge. Careful studies have shown that the absorption edge is actually described by a linear superposition of $[\omega - \omega_{1s}(o) - \omega(\Gamma)]^{1/2}$ functions with several different $\omega(\Gamma)$ resulting from participation of different Γ phonons. Here, we shall discuss only the RRS results obtained with the exciting laser frequency tuned over the yellow exciton lines and the continuum near the absorption edge.

Experimental Arrangement and Simple Theoretical Background for RRS

We used a CW dye laser pumped by an argon ion laser as the exciting source. The dye laser could be tuned from 5250 Å to 6500 Å with a half-width $\lesssim$ 0.1 Å and a typical output power $>$ 30 mW. A double monochromator

and a photon counting system were used in the detection of scattered radiation. The sample was kept in superfluid He bath at ~ 2°K. The Raman spectrum was normalized against the intensity of a Raman line of calcite measured under similar condition.

Strictly speaking, Stokes emission in RRS has contributions from both resonant fluorescence and resonant scattering, and the theoretical expression is in general quite complicated.[8] However, in simple cases where lifetime broadening dominates the linewidths, one finds that the total resonant Stokes emission cross-section σ_R for a Raman mode is given by a simple relation[8,9]

$$\sigma_R = (\text{Absorption Cross-section}) \times (\text{Quantum Efficiency of Stokes emission}). \quad (1)$$

In the following sections, we shall always use Eq. (1) to discuss our results.

<u>One-Phonon RRS Near the 1s Yellow Exciton in Cu_2O</u>.

We want to find out how RRS varies when the exciting laser frequency ω_ℓ scans over the absorption spectrum in Fig. 3a. We first consider the case where ω_ℓ is near the 1s yellow exciton line. The experimental results of Compaan and Cummins[3] are presented in Figs. 4 and 5. The Raman spectra in Figs. 4a and 4b were obtained respectively with ω_ℓ on and off resonance with the 1s yellow exciton line. The on-resonance spectrum has the appearance of a set of new lines which

correspond to the forbidden one-phonon modes. The RRS enhancement of the Γ_{12}^{-} modes is shown in Fig. 5.

The results can be easily understood. The RRS process can be considered as excitation of the 1s yellow exciton followed by emission of a Stokes photon and a phonon. The exciton is excited by electric-quadrupole transition. Since the exciton has the same parity as the ground state of the system, the phonon-assisted recombination of the exciton must involve an odd-parity, and hence Raman-forbidden, zone-center phonon mode. The results in Fig. 5 agree well with the prediction of Eq. (1). Let $\alpha(\omega_\ell)$ be the absorption cross-section of the electric-quadrupole excitation, $\gamma_{rad}(\Gamma)$ the Γ-phonon-assisted radiative decay rate, and γ_{tot} the total decay rate of the exciton. Then, Eq. (1) becomes

$$\sigma_R(\omega_\ell,\Gamma) = \alpha(\omega_\ell)\gamma_{rad}(\Gamma)/\gamma_{tot}. \qquad (2)$$

Since $\gamma_{rad}(\Gamma)/\gamma_{tot}$ is expected to be independent of ω_ℓ near the exciton line, we then find $\sigma_R(\omega_\ell) \propto \alpha(\omega_\ell)$.

Equation (2) shows

$$\sigma_R(\omega_\ell,\Gamma)/\sigma_R(\omega_\ell,\Gamma') = \gamma_{rad}(\Gamma)/\gamma_{rad}(\Gamma').$$

The radiative decay rate $\gamma_{rad}(\Gamma)$ is directly proportional to the square of the matrix element for phonon-assisted exciton recombination. Therefore, the ratio of $\sigma_R(\omega_\ell,\Gamma)$ for different phonons can yield information about the relative coupling strength between the 1s yellow exciton and the phonons.

One-phonon RRS can also occur in the following way. The zone center 1s exciton is first excited by simultaneous absorption of a ω_ℓ photon and emission of an odd-parity phonon; the exciton then decays by emission of a Stokes photon at ω_s via electric-quadrupole transition. It is easy to show, using Eq. (1), that in this case σ_R is proportional to $\alpha(\omega_s)$.

Two-Phonon RRS Near the Absorption Edge in Cu_2O

The 1s exciton with a finite momentum ($k > \omega_\ell n/c$ away from the zone center) can also be excited via phonon-assisted transition. Neglecting the optical wave vector we find that the exciton frequency is given by

$$\omega_{1s}(\vec{k}) = \omega_{1s}(o) + \hbar k^2/2M$$
$$= \omega_\ell - \omega(\Gamma(\vec{k})) \qquad (3)$$

where M is the exciton effective mass and $\omega(\Gamma(\vec{k}))$ is the frequency of the Γ phonon with a wave vector $\vec{k}$. By momentum conservation, a $k \neq 0$ exciton cannot decay by emission of only a single photon. It can nevertheless decay by phonon-assisted transition. Phonon-assisted excitation of such an exciton followed by phonon-assisted recombination constitutes a two-phonon RRS process. Energy conservation requires

$$\omega_\ell - \omega_s = \omega(\Gamma(k)) + \omega(\Gamma'(k)) \qquad (4)$$

From Eq. (1), the two-phonon RRS cross-section is given by

$$\sigma_R = [\alpha(\Gamma)\gamma_{rad}(\Gamma'(k)) + \alpha(\Gamma')\gamma_{rad}(\Gamma(k))]/\gamma_{tot}(k) \qquad (5)$$

where $\alpha(\Gamma)$ is the absorption cross-section for phonon-assisted excitation of the ls exction at $\omega_{ls}(k)$ and $\gamma_{rad}(\Gamma(k))$ is the phonon-assisted radiative decay rate of the exciton. It can easily be shown that for dispersionless phonon,

$$\alpha(\Gamma) \propto [\omega_\ell - \omega_{ls}(o) - \omega(\Gamma)]^{1/2} \quad \text{if} \quad \omega_\ell > \omega_{ls}(o) + \omega(\Gamma)$$

$$= 0 \text{ otherwise.} \qquad (6)$$

In Eq. (5), $\gamma_{rad}(\Gamma)$ is directly proportional to the square of the phonon-assisted transition matrix element and should be nearly independent of $\omega_{ls}(k)$. However, since $k \neq o$, the total exciton decay rate γ_{tot} is no longer a constant but is a strong function of $\omega_{ls}(k)$. Physically, excitons with higher energies have more lower energy states to decay into and hence the decay rate is higher. Taking into account only the relatively stronger exciton decay mechanisms, we can write[2]

$$\gamma_{tot}(k) = A + B[\omega_\ell - \omega_{ls}(o) - \omega(\Gamma_{12}^-)] + C[\omega_\ell - \omega_{ls}(o) - 3\omega(\Gamma_{12}^-)]$$
$$+ \text{---} \qquad (7)$$

where A, B, C are constants; the first term is due to scattering by defects and impurities, direct radiation, and optical-phonon-assisted radiation; the second term is due to emission of an LA phonon; the third term is due to simultaneous emission of two Γ_{12}^{-} phonons; etc. Equation (7) shows that γ_{tot} increases as ω_ℓ increases. Thus from Eqs. (5) - (7), we expect that σ_R for two-phonon RRS should first increase sharply at $\omega_\ell \sim \omega_{1s}(o) + \omega(\Gamma)$ and then drops off more gradually with increasing ω_ℓ. A number of sharp lines in Fig. 2 correspond to two-phonon Raman modes. Experimental results on RRS by two Γ_{12}^{-} phonons at 220 cm^{-1} near the absorption edge are presented in Fig. 6 as an example. The results on other two-phonon modes are similar. The dashed curve in Fig. 6 was obtained by calculating $\sigma_R(\omega_\ell)$ from Eqs. (5) - (7) using appropriate values for A, B, and C.[2] It is seen that the theoretical curve is in good agreement with the experimental results.

The agreement between theory and experiment gives the following affirmative information. 1) The observed optical absorption edge is indeed due to phonon-assisted excitation of 1s yellow excitons. 2) Various steps at the absorption edge are identified as due to phonon-assisted transitions involving various phonon modes. 3) The two-phonon modes in the Raman spectrum are unambiguously identified through their resonant behavior. 4) The relative coupling strengths between exciton and various phonons can be deduced from the intensity ratios of the different two-phonon modes. 5) The exciton lifetime ($= 1/\gamma_{tot}$) is an energy-dependent quantity.

It is also possible to deduce phonon dispersion from two-phonon RRS.[4] Equations (3) and (4) show that the Raman shift $(\omega_\ell - \omega_s)$ is a function of k and hence ω_ℓ. If the phonons emitted are dispersionless, then $\omega_\ell - \omega_s$ is independent of ω_ℓ. This is true for most of the two-phonon modes in Cu_2O. However, the $\Gamma_{15}^{-(1)}$(LO) mode is fairly dispersive, and therefore the frequency of the $\Gamma_{12}^- + \Gamma_{15}^{-(1)}$(LO) mode has a clear dependence on ω_ℓ, as shown in Fig. 7. From Eqs. (3) and (4), if the exciton effective mass M is known, then since Γ_{12}^- is dispersionless, the dispersion of $\Gamma_{15}^{-(1)}$(LO) can be easily calculated. With $M = 3m_o$ where m_o is the electron mass, we have found good agreement on the dispersion of $\Gamma_{15}^{-(1)}$(LO) between our measured value and the theoretical value of Carabatos and Prevot.[10]

In Fig. 7, there are another three strongly dispersive modes which split off from the $2\Gamma_{12}^-$ mode as $\omega_\ell \gtrsim \omega_{1s}(o) + \omega(\Gamma_{12}^-)$. These are modes connected with $2\Gamma_{12}^-$ + acoustic phonons.[4]

RRS of $2\Gamma_{12}^-$ + Acoustic Phonons in Cu_2O

The exciton at $\omega_{1s}(k)$ excited by Γ_{12}^- - phonon-assisted absorption can first decay into a lower excitonic state at $\omega_{1s}(k')$ by emitting one or several acoustic phonons and then radiatively recombine with emission of another Γ_{12}^- phonon. The RRS cross-section for $2\Gamma_{12}^- + TA(\omega_{TA})$ is

$$\sigma_R(\omega_\ell, 2\omega_{\Gamma_{12}^-} + \omega_{TA}) = \alpha(\Gamma_{12}^-)[\gamma_{TA}(k,\omega_{TA})/\gamma_{tot}][\gamma_{rad}(\Gamma_{12}^-)/\gamma_{tot}] \quad (8)$$

where $\gamma_{TA}(k,k')$ is the exciton decay rate from $\omega_{1s}(k)$ to $\omega_{1s}(k')$ through emission of a transverse acoustic phonon and can be calculated.[4] With ω_ℓ fixed, Eq. (8) describes the Raman lineshape of the $2\Gamma_{12}^-$ + TA mode. The solid curve in Fig. 7 is a plot of $[\sigma(\omega_\ell, 2\omega_{\Gamma_{12}^-} + \omega_{TA})]_{max}$ versus ω_ℓ, obtained from Eq. (8) by assuming $M = 3m_o$. It agrees well with the experimental data.

Similarly, we can find $\sigma_R(\omega_\ell, 2\omega_{\Gamma_{12}^-} + \omega_{LA})$ for the $2\Gamma_{12}^-$ + LA(ω_{LA}) mode. The solid curve Y in Fig. 7 is a theoretical plot of $[\sigma_R(\omega_\ell, 2\omega_{\Gamma_{12}^-} + \omega_{LA})]_{max}$ versus ω_ℓ, assuming again $M = 3m_o$. It has a stronger dependence on ω_ℓ since the LA phonon has a larger dispersion than TA. We also found experimentally

$$\frac{\sigma_R(2\omega_{\Gamma_{12}^-} + \omega_{LA})}{\sigma_R(2\omega_{\Gamma_{12}^-} + \omega_{TA})} = \frac{\gamma_{LA}(\omega_{LA})}{\gamma_{TA}(\omega_{TA})} \simeq 45.$$

This actually corresponds to the ratio of the square of the matrix elements for exciton -LA and exciton -TA phonon coupling.

Because of the stronger exciton -LA -phonon coupling, even the $2\Gamma_{12}^-$ + 2LA mode was detectable. The calculated $[\sigma_R(\omega_\ell, 2\omega_{\Gamma_{12}^-} + 2\omega_{LA})]_{max}$ versus ω_ℓ is shown as the solid Z curve in Fig. 7. The quantitative agreement between theory and experiment in all these cases suggests that our choice of the exciton effective mass $M = 3m_o$ is indeed correct.

RRS of Three and Four Phonons in Cu_2O.[4]

The exciton at $\omega_{1s}(k)$ can also first decay into a lower excitonic state by emitting one or several optical phonons and then radiatively

recombine with emission of another optical phonon. For example, the RRS cross-section for the $3\Gamma_{12}^-$ mode is

$$\sigma_R(3\Gamma_{12}^-) = \alpha(\Gamma_{12}^-)[\gamma_p(\Gamma_{12}^-)/\gamma_{tot}][\gamma_{rad}(\Gamma_{12}^-)/\gamma_{tot}] \qquad (9)$$

where $\gamma_p(\Gamma_{12}^-)$ is the exciton decay rate from $\omega_{1s}(k)$ to $\omega_{1s}(k')$ through emission of a Γ_{12}^- phonon. Since the lowest exciton state is at $\omega_{1s}(o)$, we must have $\omega_{1s}(k) \geq \omega_{1s}(o) + \omega(\Gamma_{12}^-)$. Then from Eq. (3), we find $\omega_\ell \geq \omega_{1s}(o) + 2\omega(\Gamma_{12}^-)$ as the threshold frequency for observing RRS of the $3\Gamma_{12}^-$ mode. Figure 8 shows the RRS enhancement of a number of 3-phonon modes. In each case, the Raman cross-section increases sharply at a predicted threshold frequency.

RRS by four Γ_{12}^- phonons has also been observed. The RRS cross-section is

$$\sigma_R(4\Gamma_{12}^-) = \alpha(\Gamma_{12}^-)[\gamma_p(2\Gamma_{12}^-)/\gamma_{tot}][\gamma(\Gamma_{12}^-)/\gamma_{tot}]. \qquad (10)$$

Again, we expect $\gamma_p(2\Gamma_{12}^-) \neq 0$ only if $\omega_\ell \geq \omega_{1s}(o) + 3\omega(\Gamma_{12}^-)$. This threshold condition was indeed observed as shown in Fig. 8.

Two-Phonon RRS Around the Excited Yellow Exciton States.[4]

We can also have RRS with ω_ℓ or ω_s near resonance with the np excited states of the yellow exciton. Electric-dipole excitation of the np exciton states is allowed. RRS can occur, for example, with the

excitation of an exciton in the np state followed by emission of two odd-parity phonons and a Stokes photon. Since the excitonic states are sharp, the RRS enhancement is also expected to be sharp. Figure 9 shows an example of two-phonon RRS with ω_ℓ near resonance with the np yellow exciton states. The experimental results agree well with the solid curve in the figure obtained theoretically from the prescribed scattering mechanism given in the inset.[4]

Two-Magnon RRS in MnF_2.[5]

The principles of two-phonon RRS near the phonon-assisted absorption edge in Cu_2O can be applied to two-magnon RRS in MnF_2. Figure 10 shows the absorption spectrum of MnF_2 between 18400 and 18500 cm^{-1}. We shall discuss here only the case where the polarizations are perpendicular to the $\hat{c}$-axis. In the figure, E_1 and E_2 have been identified as the exciton lines and σ_1 and σ_2 as the corresponding magnon sidebands. The exciton and magnon dispersion curves are sketched in the inset of Figure 10.

In the two-magnon RRS process, an exciton at $\omega_{1s}(k)$ is excited by magnon-assisted optical absorption followed by emission of a Stokes photon and another magnon. We therefore expect to observe resonant enhancement when ω_ℓ falls within the magnon sidebands σ_1 and σ_2. From energy conservation, we have

$$\omega_\ell = \omega_{ex}(k) + \omega_{mag}(k)$$
$$= \omega_s + 2\omega_{mag}(k) \qquad (11)$$

This indicates that the Raman shift $\omega_\ell - \omega_s$ now depends on ω_ℓ and is a linear function of ω_ℓ if the excitonic dispersion can be neglected. This linear relation is represented in Fig. 11a by the dashed lines for the two excitons E_1 and E_2. They describe a portion of the two-magnon Raman shift data very well. The disagreement between theory and experiment away from the magnon sidebands is due to contribution from the nonresonant two-magnon Raman scattering.[11] As expected, the Raman shift determined from Eq. (11) is only valid when the resonant contribution dominates. Deviation on the high energy side close to a peak of a magnon sideband is preseumably due to the strong dominance of the resonance enhancement near the zone edge.

It is easy to show that the two-magnon Raman cross-section is given by[5]

$$\sigma = \sigma_R + \sigma_{NR} \qquad (12)$$

where the resonant part is related to the nonresonant part by

$$\sigma_R \propto d\sigma_{NR}(\omega_\ell - \omega_s = 2\omega_\ell - 2\omega_{1s})/d\omega_s. \qquad (13)$$

The solid curves in Fig. 10b are obtained from Eqs. (12) and (13) using the experimental lineshape of $d\sigma_{NR}/d\omega_s$ and with σ_R normalized to its peak value. They describe the experimental data very well.

Conclusion.

We have used RRS in Cu_2O and in MnF_2 as examples to illustrate how powerful the resonant Raman technique is. It is shown that from RRS measurements, one can have a better understanding of the phonon or magnon structure of the crystal, and in addition, obtain information about the excitonic properties and exciton-phonon (Magnon) coupling. The ideas and basic principles discussed here can be extended to electron-hole pairs and to other elementary excitations. For example, one-phonon and two-phonon RRS near the absorption edge of a crystal can presumably help in determining whether the energy gap is direct or indirect; and in some magnetic crystals, one may expect to observe RRS by a magnon-phonon pair near a phonon or magnon sideband.

Acknowledgement

This work was sponsored by the U. S. Energy Research and Development Administration.

REFERENCES

1. See, for example, E. F. Gross, J. Phys. Chem. Solids 8, 172 (1959); Adv. Phys. Sci. (Moscow) 76, 432 (1962).

2. P. Y. Yu, Y. R. Shen, Y. Petroff, and L. Falicov, Phys. Rev. Lett. 30, 283 (1973).

3. A. Compaan and H. Z. Cummins, Phys. Rev. Lett. 31, 41 (1973).

4. P. Y. Yu and Y. R. Shen, Phys. Rev. Lett. 32, 373 (1974); Phys. Rev. Lett. 32, 939(1974); Phys. Rev. (1975, to be published).

5. N. M. Amer, T. C. Chiang, and Y. R. Shen, Phys. Rev. Lett. 34, 1454 (1975).

6. J. Reydellet, M. Balkanski, and D. Trivich, Phys. Stat. Solidi 52b, 175 (1972).

7. R. J. Elliot, Phys. Rev. 124, 340 (1961).

8. Y. R. Shen, Phys. Rev. B9, 622 (1974).

9. M. V. Klein, Phys. Rev. B8, 919 (1973).

10. C. Carabatos and B. Prevot, Phys. Stat. Solidi 44, 70 (1971).

11. P. A. Fleury, S. P. S. Porto, and R. Loudon, Phys. Rev. Lett. 18, 658 (1967).

FIGURE CAPTIONS

Fig. 1. Crystal structure of Cu_2O.

Fig. 2. Off-resonance Raman spectrum of Cu_2O obtained with a Kr ion laser at 6471 Å (after Ref. 6).

Fig. 3(a) Sketch of absorption spectrum of Cu_2O near the absorption edge

(b) Sketch of the two top valence and two bottom conduction bands near the center of the Brillouin zone.

Fig. 4. Raman spectra of Cu_2O at low temperature (a) Laser frequency 10 cm^{-1} above the 1s yellow exciton frequency. (b) Laser frequency in resonance with the 1s yellow exciton. The features labelled L are due to phonon-assisted luminescence. (after Ref. 3)

Fig. 5. Resonance enhancement of the 109-cm^{-1} Γ_{12}^- Raman line in comparison with the nonresonant behavior of the 218-cm^{-1} $2\Gamma_{12}^-$ Raman line. (after Ref. 3)

Fig. 6. The Raman cross-section of the $2\Gamma_{12}^-$ mode of Cu_2O plotted as a function of incident photon energies. The broken line is a plot of Eq. (5). (after Ref. 2)

Fig. 7. Raman frequency shifts of all the observes Raman modes of Cu_2O between 190 and 400 cm^{-1} as a function of incident photon energy ω_ℓ. The broken curves are drawn for clarity. The solid curves are theoretical curves discussed in the text. The vertical bars over the experimental points indicate the half-widths of the corresponding Raman peaks. The position of the absorption edge at $\omega_{1s}(o) + \omega(\Gamma_{12}^-)$ is indicated by an arrow. (after Ref. 4)

Fig. 8. Raman cross-sections of three- and four-phonon modes of Cu_2O plotted as a function of incident photon frequencies: ...+....+ ....$2\Gamma_{12}^- + \Gamma_{25}^-$ mode, -.-o.-o.-$3\Gamma_{12}^-$ mode $\Delta\ \Delta\ \Delta$ $2\Gamma_{12}^- + \Gamma_{15}^{-(1)}$ mode and ...o...o....$4\Gamma_{12}^-$ mode. The solid line is a theoretical curve. (after Ref. 4)

Fig. 9. (a) Absorption spectrum of Cu_2O measured at ~ 5°K. The dashed curve represents the background absorption due to phonon-assisted transitions. (b) Raman cross-section of the $\Gamma_{15}^{-(2)}(L) + \Gamma_{12}^{-}(770cm^{-1})$ mode of Cu_2O obtained at ~ 10°K as a function of incident photon energies. The solid curve is the theoretical curve [Eq.(6)]. (c) Schematic diagram of the dominant resonant Raman process at $\omega_\ell \sim \omega_{3p}$. g stands for the ground state; β, for an allowed exciton. (after Ref. 4)

Fig. 10. Absorption spectrum of MnF_2 at 1.6K between 18 400 and 18 500 cm^{-1}. The solid and the dashed curves are for polarizations perpendicular and parallel to the $\hat{c}$ axis, respectively. The inset is a sketch of the relevant energy levels. (after Ref. 5)

Fig. 11. (a) Two-magnon Raman shift and (b) two-mangnon Raman cross-section as functions of the excitation frequency ω_ℓ. The exciting and the scattering radiations are polarized along $\hat{y}$ and $\hat{x}$, respectively ($\hat{x}$, $\hat{y} \perp \hat{c}$). (after Ref. 5)

TABLE I. PHONON ENERGIES OF Cu_2O OBTAINED BY VARIOUS TECHNIQUES

Symmetry Assignment of Phonons		Phonon Energies (cm^{-1}) Obtained by			
		Infrared Absorption (Room Temp.)	Optical Absorption	Raman Scattering	Luminescence
			(Liquid Helium Temp.)		
Γ_{25}^-	(Silent)		88	86	87
Γ_{12}^-	(Silent)		110	109	110
$\Gamma_{15}^{-(1)}$ (TO)	(Infrared)	146.3		153	152
$\Gamma_{15}^{-(1)}$ (LO)	(Infrared)	149.3			152
Γ_2^-	(Silent)			350	350
Γ_{25}^+	(Raman)			515	515
$\Gamma_{15}^{-(2)}$ (TO)	(Infrared)	609		640	633
$\Gamma_{15}^{-(2)}$ (LO)	(Infrared)	638		660	662

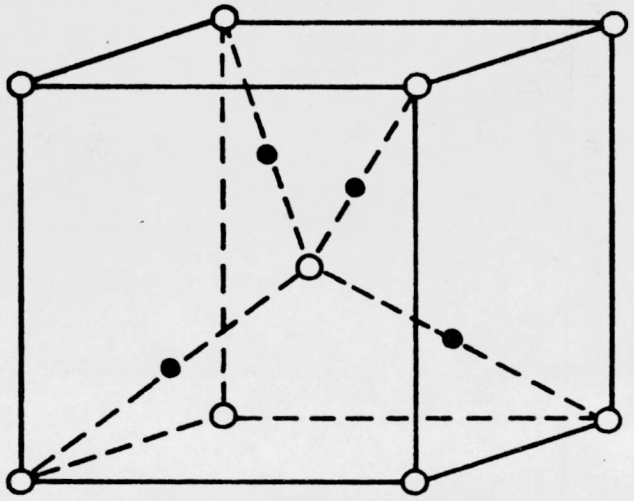

○ Oxygen

● Copper

XBL 745 813

Fig. 1

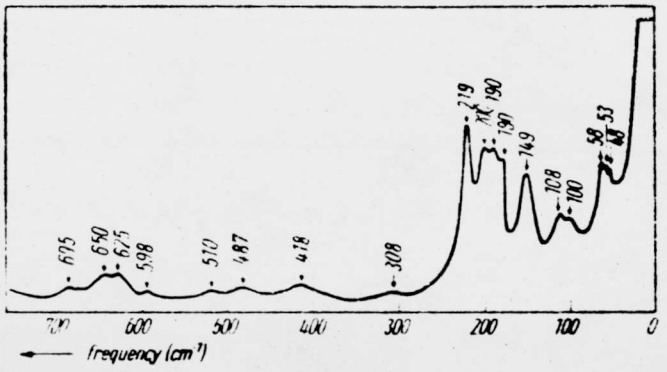
675
650
625
598
510
487
418
308
219
190
180
149
108
100
58
53
700
600
500
400
300
200
100
0
frequency (cm⁻¹)

Fig. 2

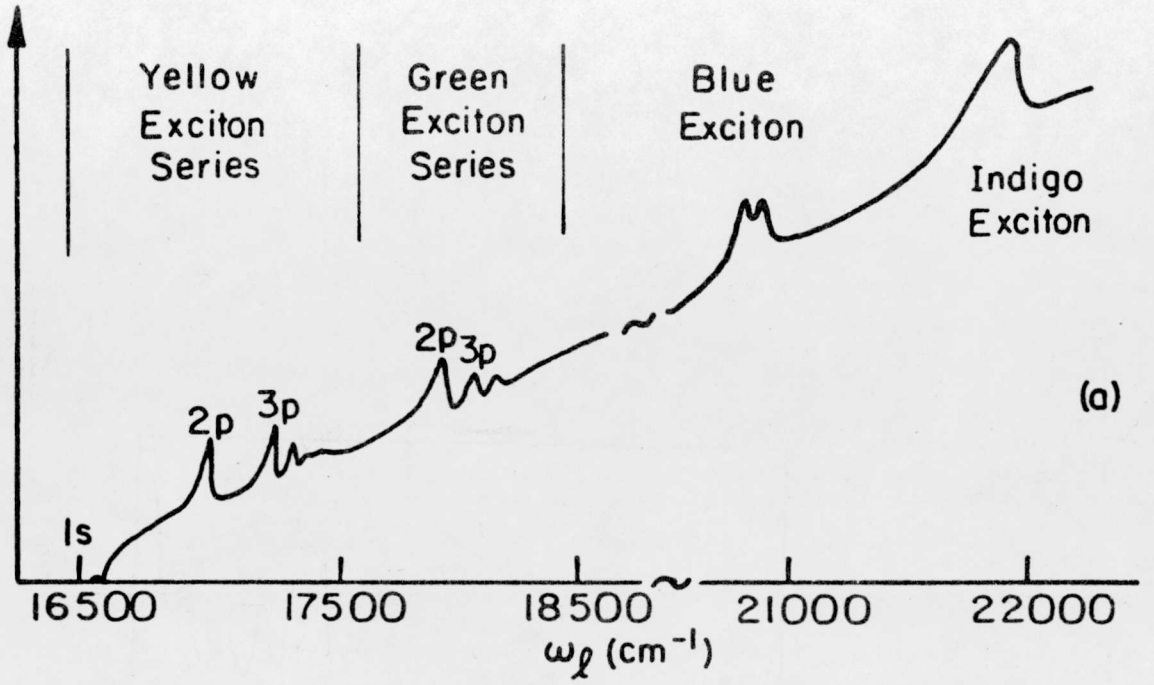

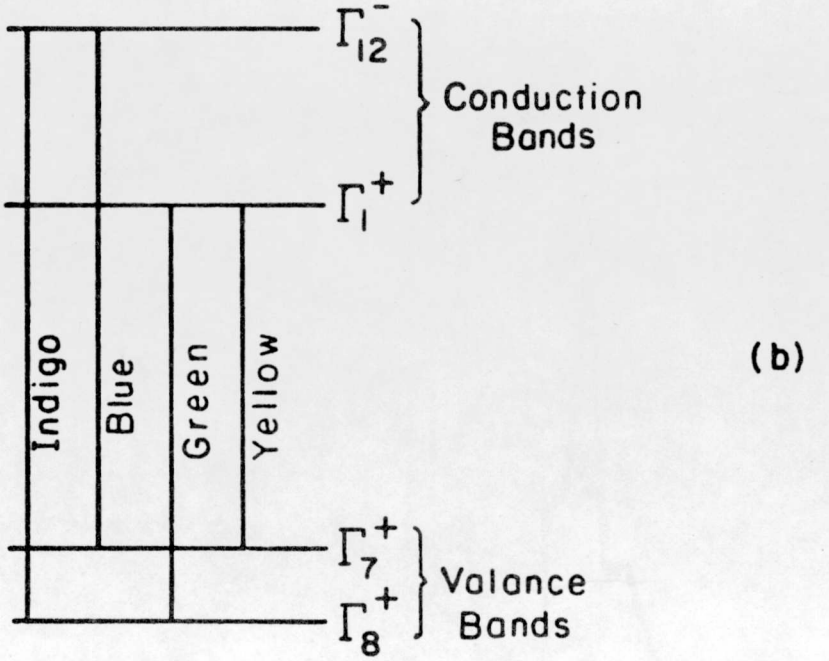

XBL 759-7330

Fig. 3

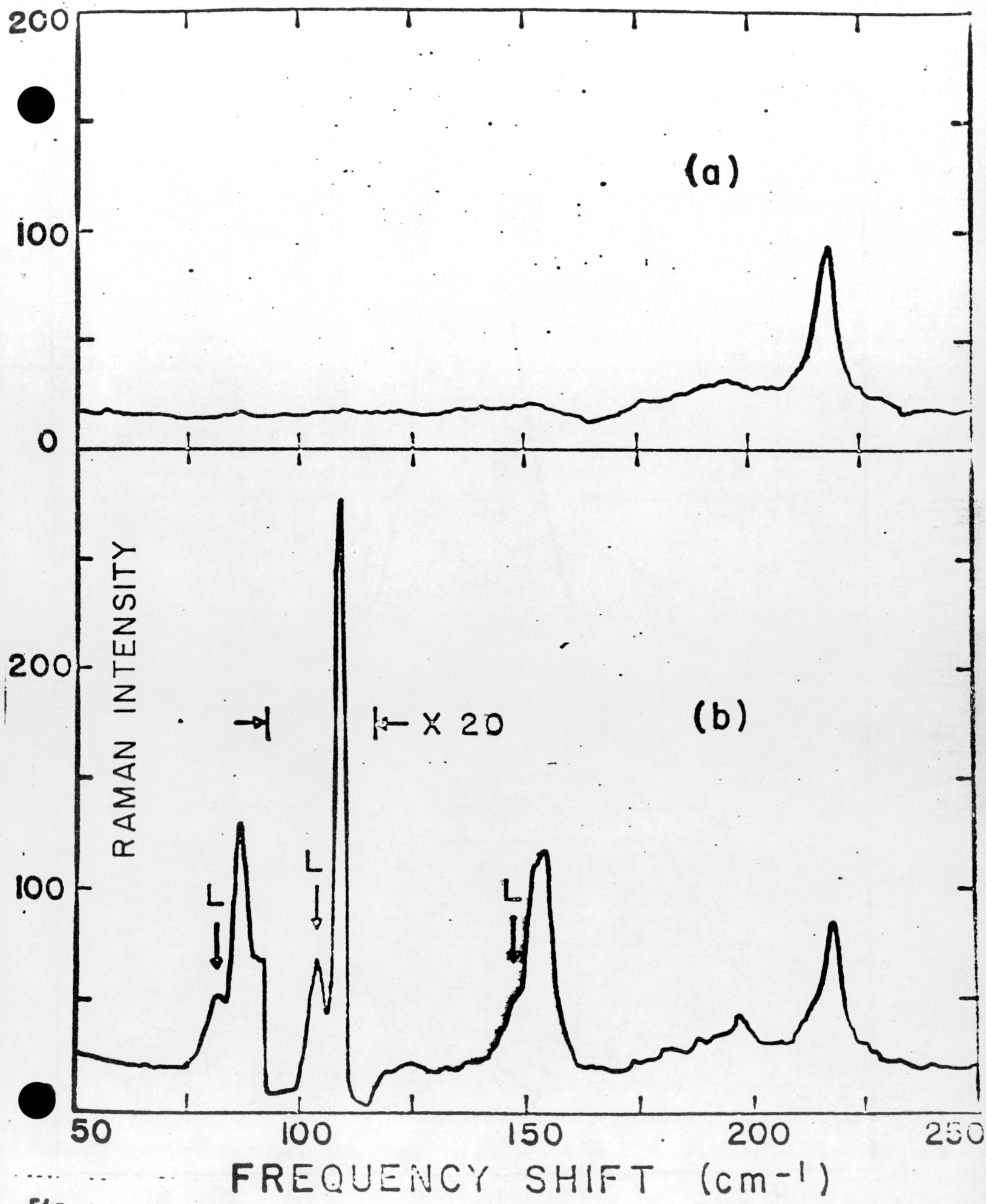
200
100
0
(a)
200
100
RAMAN INTENSITY
X 20
(b)
L
L
L
50
100
150
200
250
FREQUENCY SHIFT (cm⁻¹)

Fig. 4

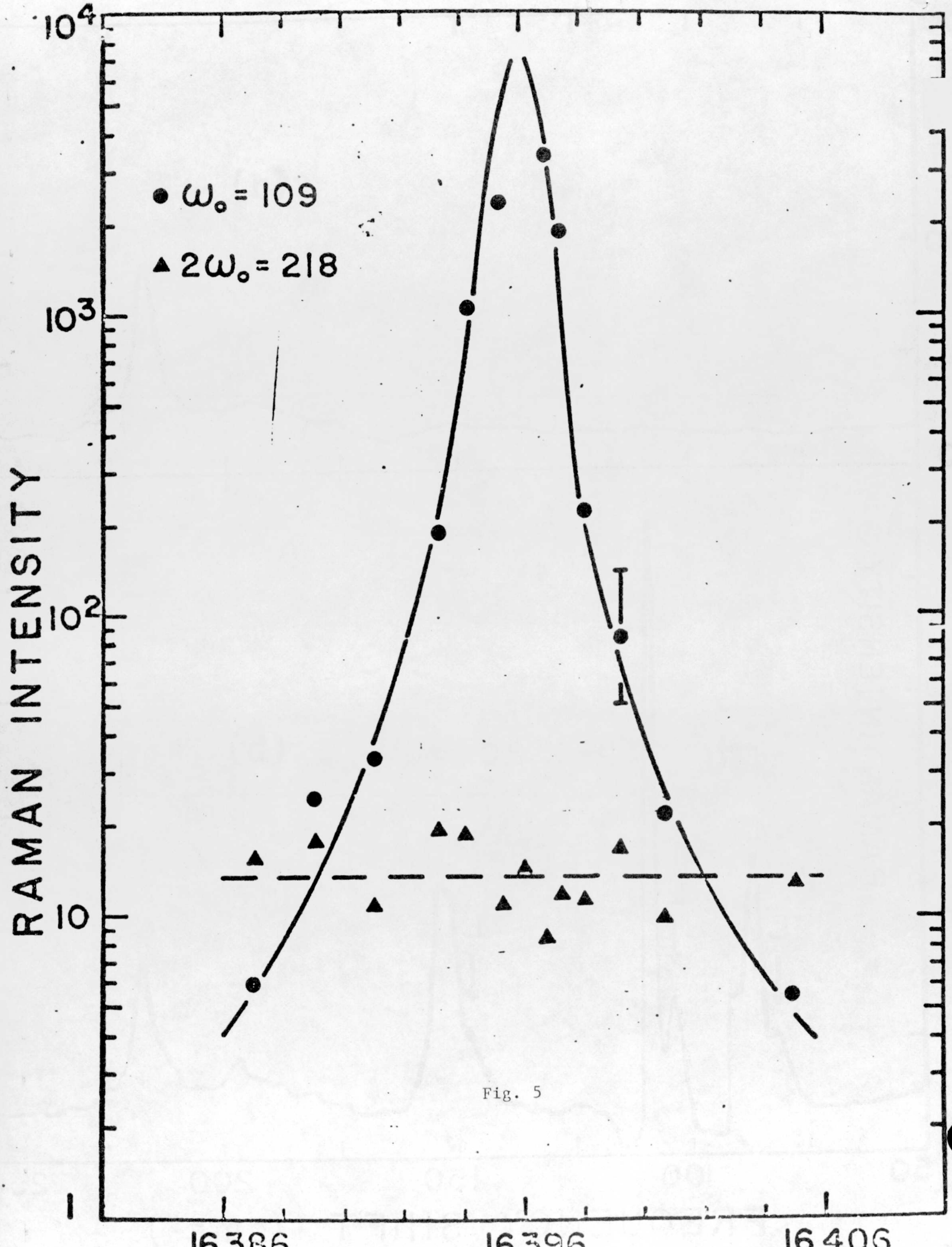
10^4
10^3
10^2
10
1
RAMAN INTENSITY
● ω_o = 109
▲ $2\omega_o$ = 218
16386
16396
16406
LASER FREQUENCY (cm-1)

Fig. 5

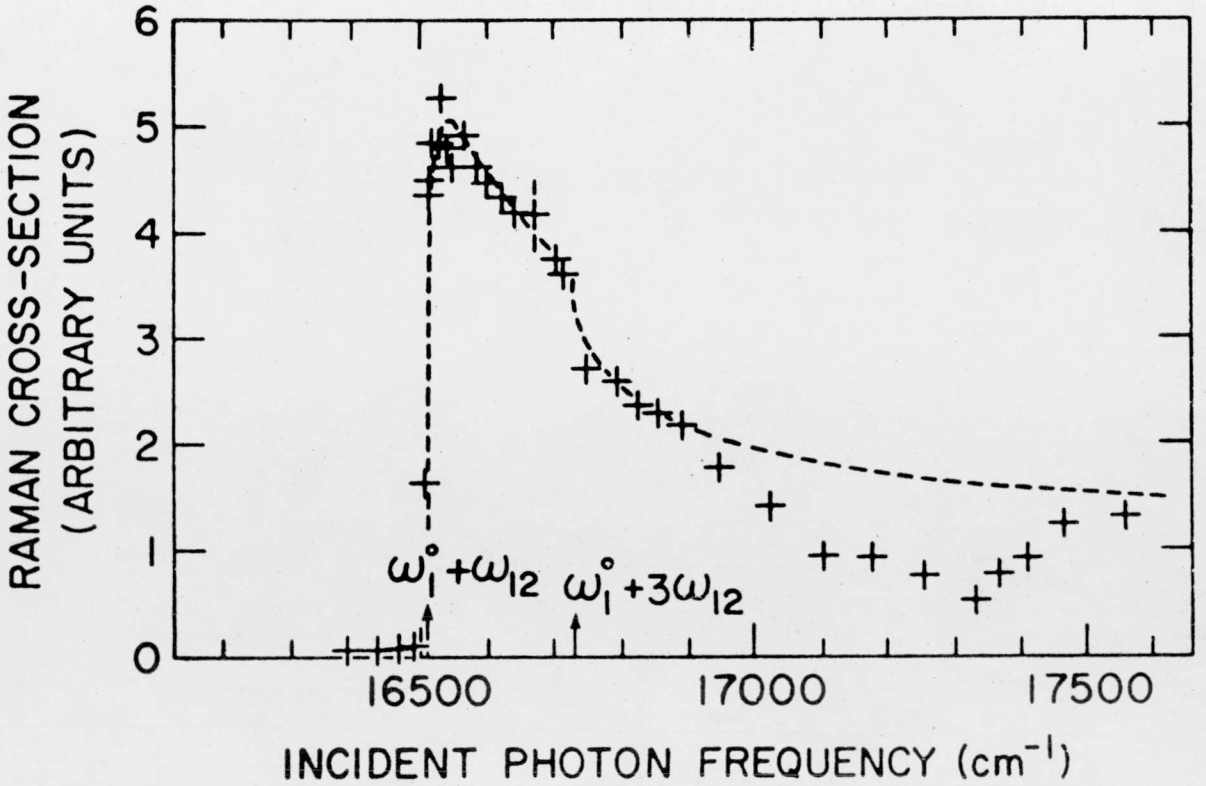
RAMAN CROSS-SECTION
(ARBITRARY UNITS)
0
1
2
3
4
5
6
16500
17000
17500
INCIDENT PHOTON FREQUENCY (cm⁻¹)
ω₁° + ω₁₂
ω₁° + 3ω₁₂

Fig. 6

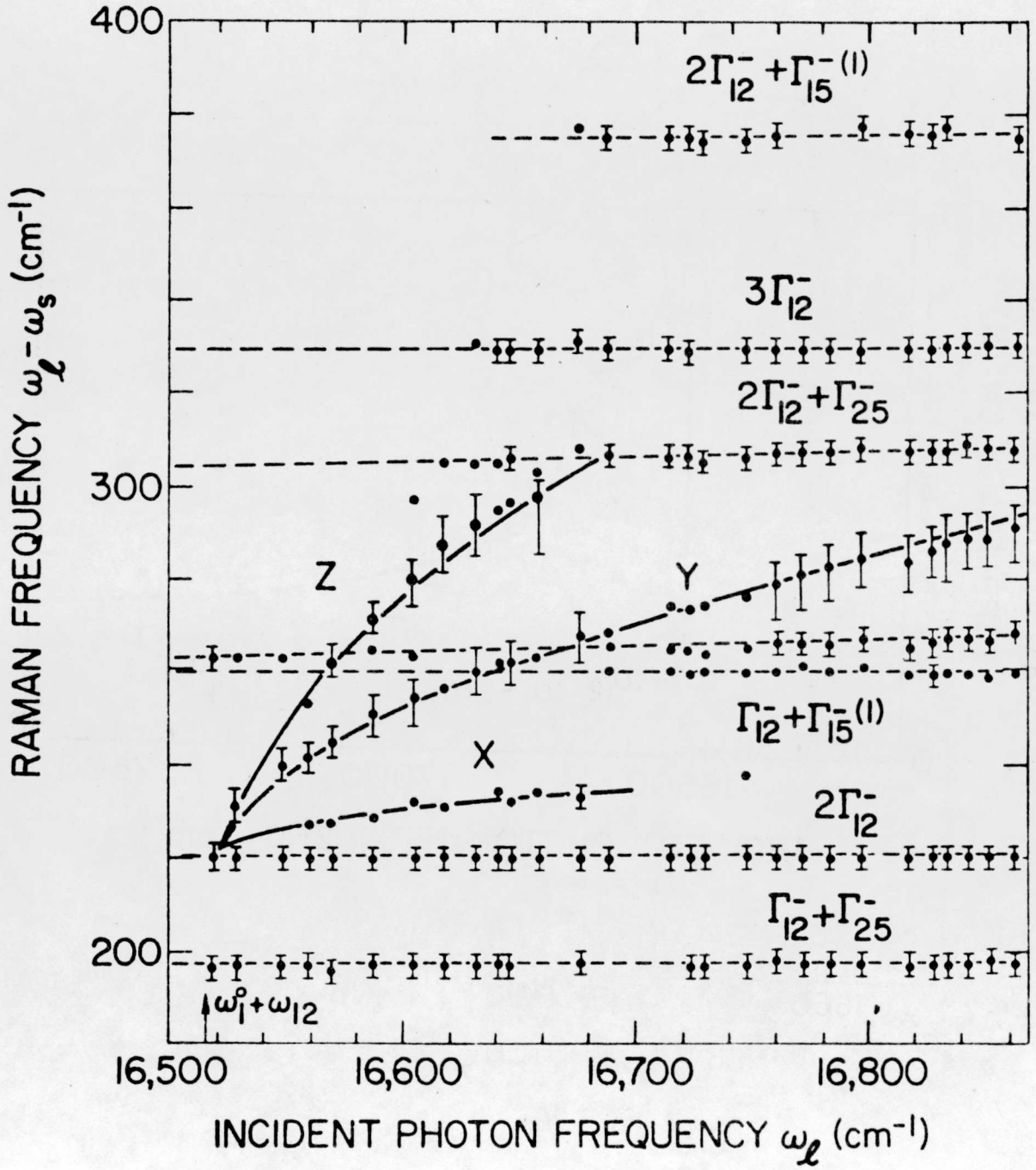
400
300
200
RAMAN FREQUENCY $\omega_\ell - \omega_s$ (cm^{-1})
$2\Gamma_{12}^- + \Gamma_{15}^{-(1)}$
$3\Gamma_{12}^-$
$2\Gamma_{12}^- + \Gamma_{25}^-$
$\Gamma_{12}^- + \Gamma_{15}^{-(1)}$
$2\Gamma_{12}^-$
$\Gamma_{12}^- + \Gamma_{25}^-$
Z
Y
X
$\omega_1^o + \omega_{12}$
16,500
16,600
16,700
16,800
INCIDENT PHOTON FREQUENCY ω_ℓ (cm^{-1})

Fig. 7

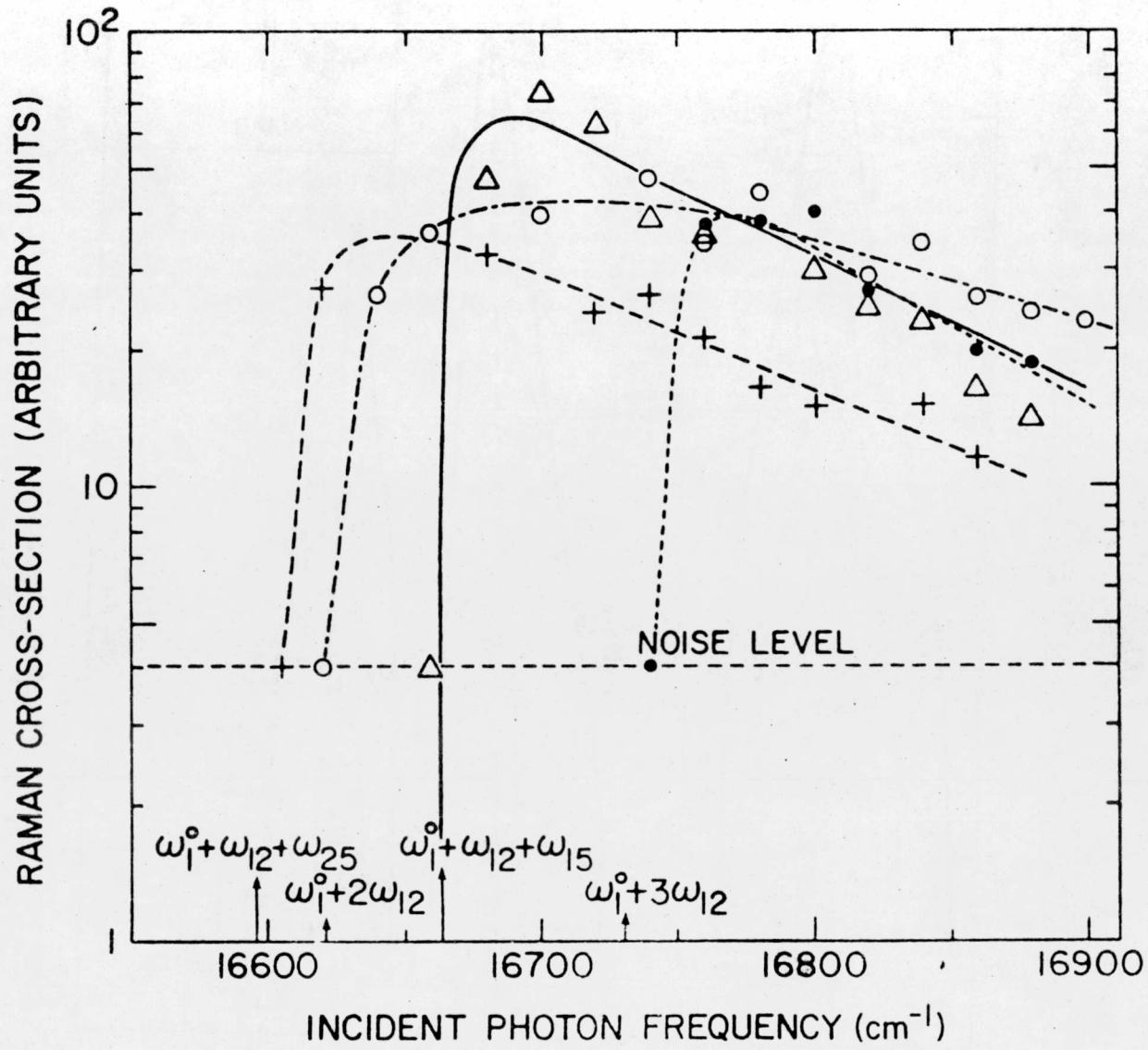
10^2
10
1
RAMAN CROSS-SECTION (ARBITRARY UNITS)
NOISE LEVEL
$\omega_1^\circ+\omega_{12}+\omega_{25}$
$\omega_1^\circ+2\omega_{12}$
$\omega_1^\circ+\omega_{12}+\omega_{15}$
$\omega_1^\circ+3\omega_{12}$
16600
16700
16800
16900
INCIDENT PHOTON FREQUENCY (cm^{-1})

Fig. 8

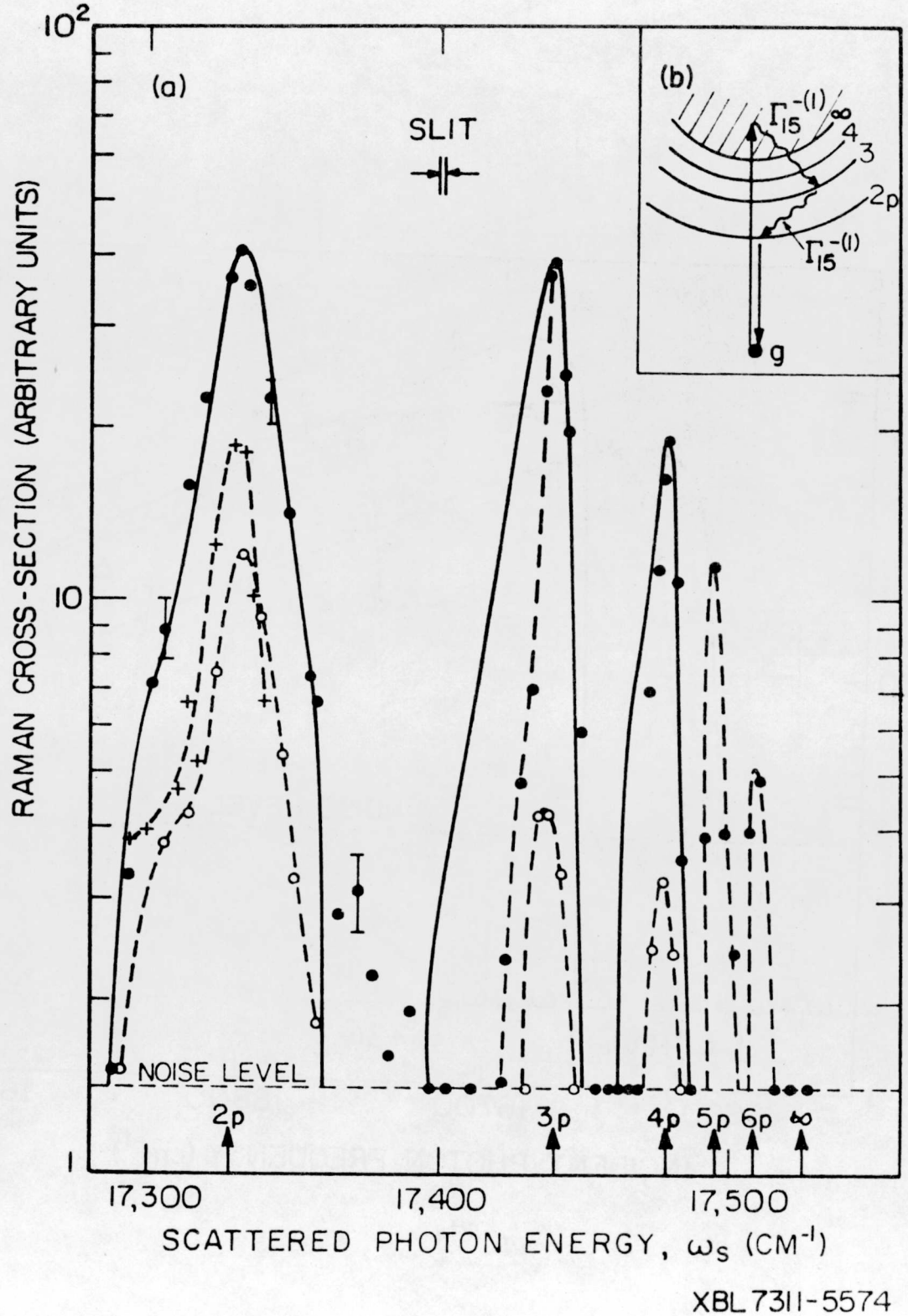
10²
10
1
RAMAN CROSS-SECTION (ARBITRARY UNITS)
(a)
SLIT
(b)
$\Gamma_{15}^{-(1)}$
∞
4
3
2p
$\Gamma_{15}^{-(1)}$
g
NOISE LEVEL
2p
3p
4p
5p
6p
∞
17,300
17,400
17,500
SCATTERED PHOTON ENERGY, ω_s (CM^{-1})
XBL 7311-5574

Fig. 9

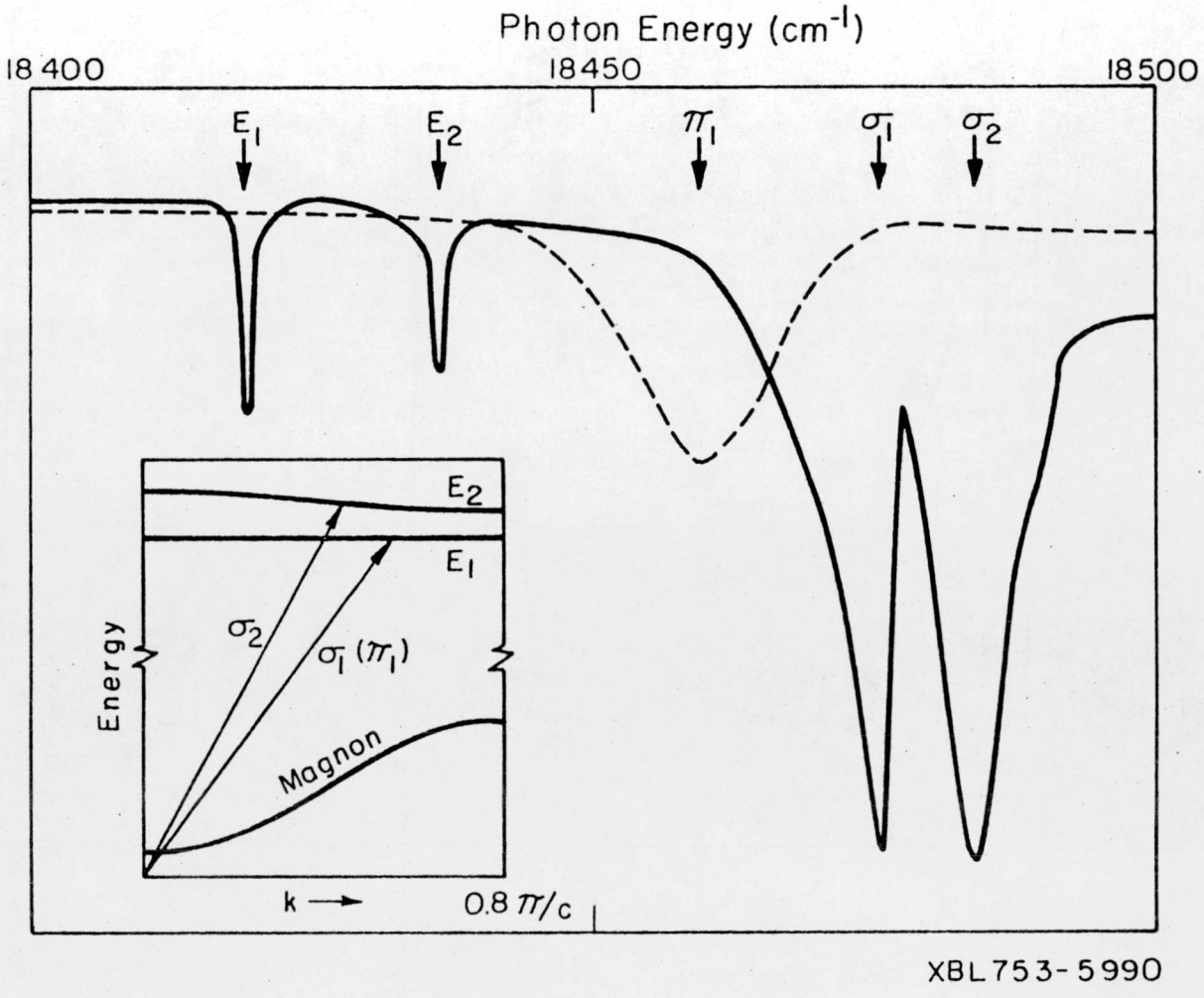
Photon Energy (cm⁻¹)
18400
18450
18500
E1
E2
π1
σ1
σ2
E2
E1
σ2
σ1 (π1)
Energy
Magnon
k →
0.8 π/c
XBL753-5990

Fig. 10

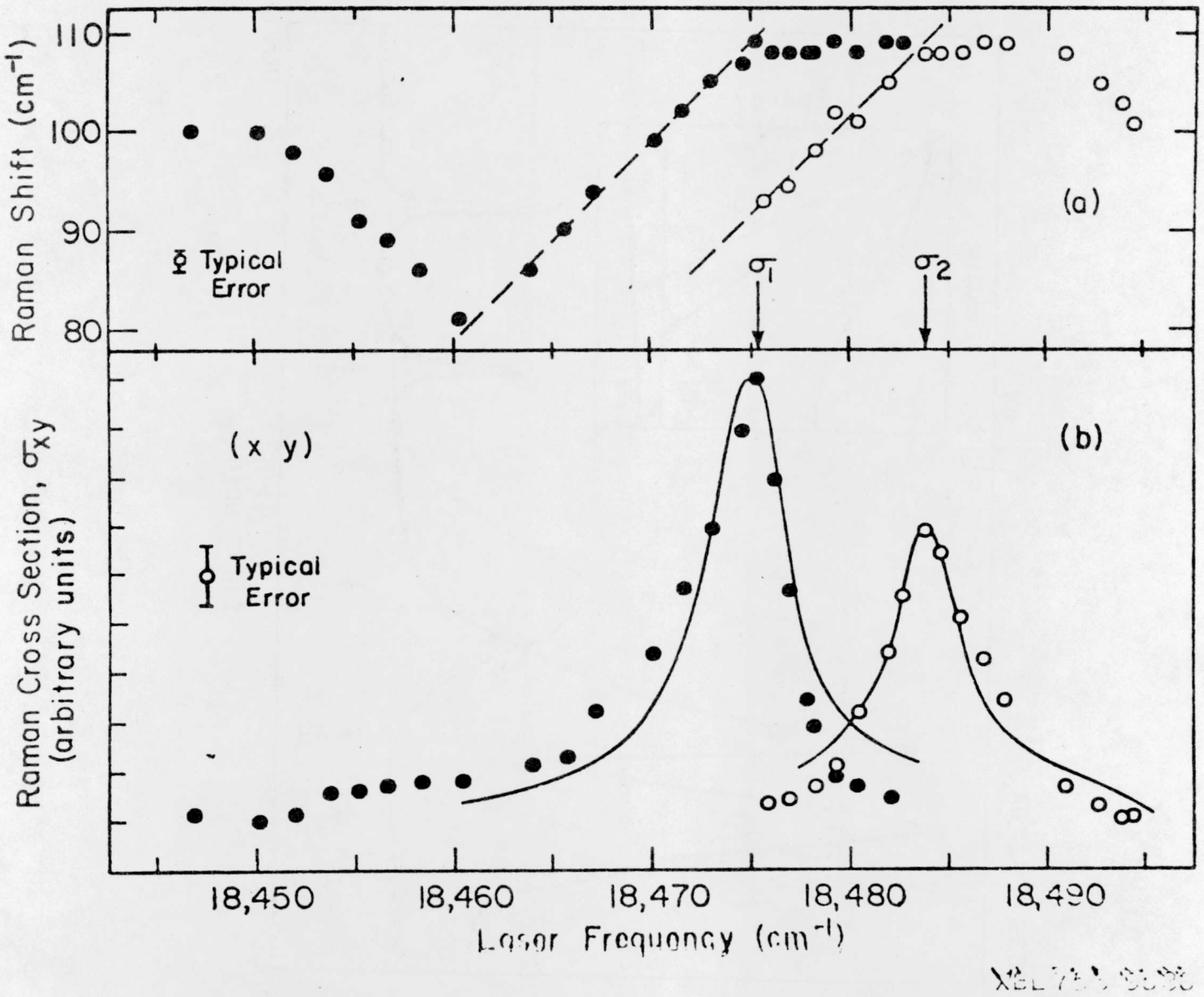
Raman Shift (cm⁻¹)
110
100
90
80
Typical Error
(a)
σ1
σ2
(x y)
(b)
Typical Error
Raman Cross Section, σxy
(arbitrary units)
18,450
18,460
18,470
18,480
18,490
Laser Frequency (cm⁻¹)

Fig. 11

TECHNICAL INFORMATION DIVISION
LAWRENCE BERKELEY LABORATORY
UNIVERSITY OF CALIFORNIA
BERKELEY, CALIFORNIA 94720